A Microfluidic Device Integrating Impedance Flow Cytometry and Electric Impedance Spectroscopy for High-Efficiency Single-Cell Electrical Property Measurement

Yongxiang Feng,[†] Liang Huang,[‡] Peng Zhao,[†] Fei Liang,[†] and Wenhui Wang*,[†]

[†]Department of Precision Instrument, Tsinghua University, Beijing, China
[‡]School of Instrument Science and Optoelectronics Engineering, Hefei University of Technology, Hefei, China

S Supporting Information

ABSTRACT: Single-cell impedance measurement is a label-free, noninvasive method for characterizing the electrical properties of single cells. At present, though widely used for impedance measurement, electric impedance flow cytometry (IFC) and electric impedance spectroscopy (EIS) are used alone for most microfluidic chips. In this paper, we present a microfluidic device combining the IFC and EIS techniques for single-cell electrical property measurement. The device uses hydrodynamic constriction to passively trap single cells and uses coplanar electrodes to obtain the impedance spectrum of the trapped cell via EIS and discrete impedance data points of the passing cells via IFC. Through experiment, we verified the individual functionality of IFC and EIS respectively, by revealing through IFC the impedance magnitude difference and quantifying through EIS the area-specific membrane capacitance and cytoplasm conductivity of the three types of cancer cells. We also demonstrated the complementarity of IFC and EIS, which holds for a wide range of the flow rate. We envision that the strategy of combining IFC and EIS provides a new thought in the efforts to enhancing the efficiency of electrical property measurement for single cells.
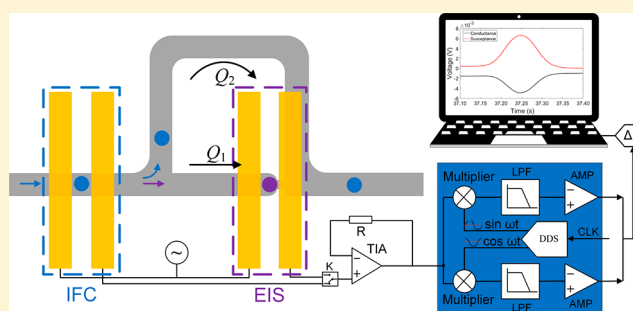
Biological cells show considerable heterogeneity, which brings single-cell analysis into recent research focus in understanding the biological process of cells.[1] Apart from proteomics, genomics, and metabolomics analysis, single-cell analysis also covers measurement of biophysical parameters.[2] Biophysical properties such as mechanical and electrical properties of cells can serve as label-free biomarkers to reveal the physiological status of cells.[3] In particular, cell electrical properties reflect the characteristics of membrane morphology, ion channel status, nuclear size, and cytoplasm.[4] For instance, red blood cells infected by plasmodium experience the change of cytoplasm conductivity and membrane permittivity.[5] So far, electrical properties have been used to characterize physiological states and distinguish different cell populations in applications including but not limited to counting,[6,7] sorting,[8] drug screening,[9] disease diagnosis,[10] and differentiation monitoring[11] and hence have gained momentum in single-cell research.[12,13]

There are many methods for cell electrical property measurement. The classic Nobel-prize-winning patch-clamping method relies on the electrode-embedded micropipette tip sealing with the cell membrane. Though it is widely used in biology, the operation is complicated and time-consuming with limited throughput.[14] Recent advances in MEMS and microfluidic techniques allow fabricating large-scale microelectrodes and microfluidic channels, which give rise to several attractive microfluidics-based methods, including electrorotation, electric impedance spectroscopy (EIS), electric cell−substrate impedance spectroscopy (ECIS), and impedance flow cytometry (IFC).[15,16] Among these techniques, ECIS is suitable for adherent cells,[17] while the other three are for suspended cells, which are of interest in this work.

The cell electrical property measurement methods work properly for particular purposes. Electrorotation, driven by dielectrophoresis (DEP) torque,[18] can evaluate electrical properties accurately using the rotation spectrum. But it is time-consuming, i.e., at least 5 min per cell,[18,19] and troublesome with complex measurement process involving handling high-conductivity DEP buffer.[16,20] IFC and EIS obtain the electrical properties of single cells through impedance measurement which is nondestructive and sensitive. Developed from Coulter counter,[21] IFC yields a limited number of frequency-dependent instantaneous impedance data points for a cell when it passes through rather than stays still on coplanar electrodes[22] or parallel facing electrodes.[23] Thanks to the high-throughput nature, IFC can give the statistical distribution of a cell population at the single-cell level. For
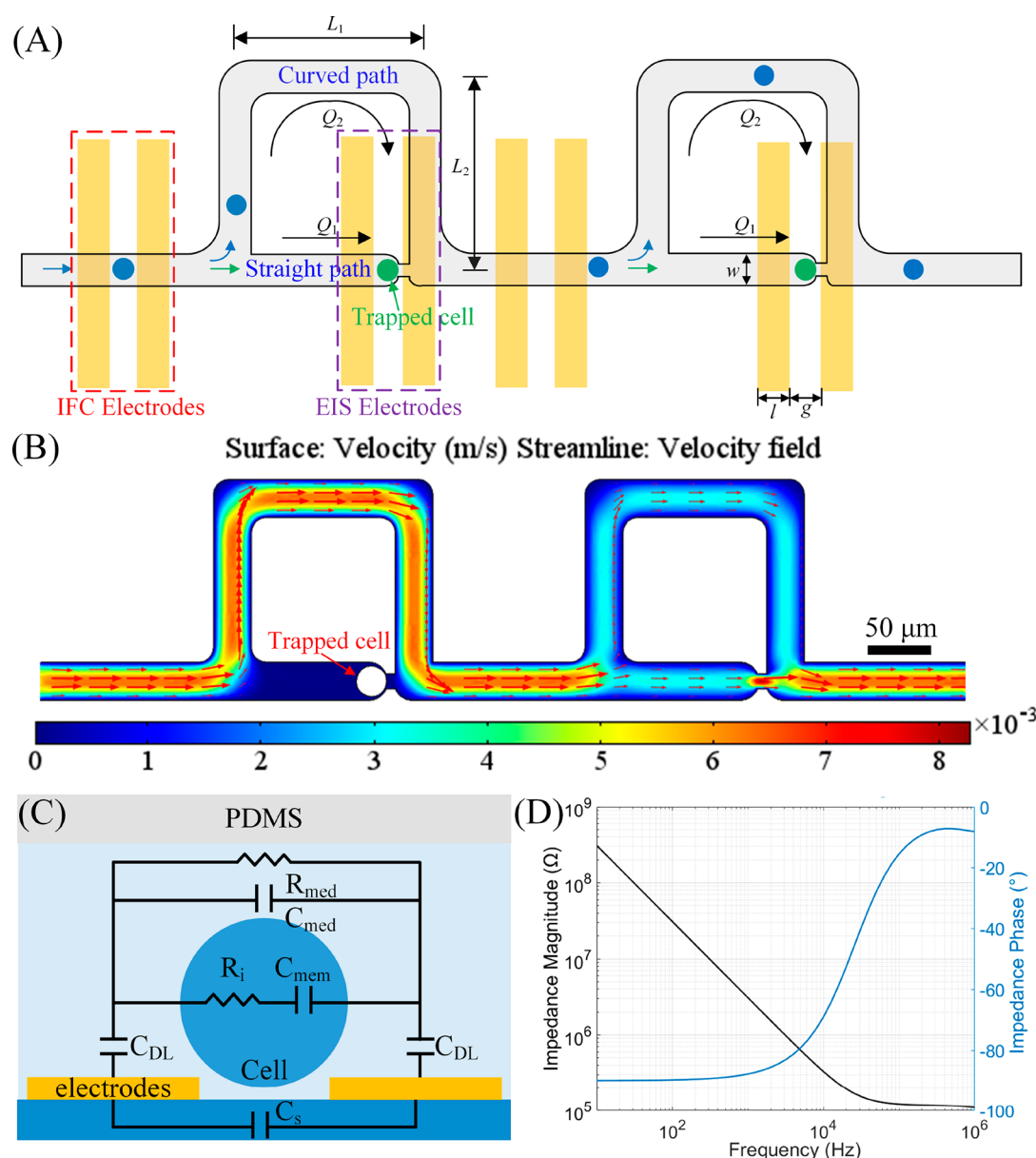
Figure 1. Device design and electrical model of single cell. (A) The schematic diagram of the microchip structure depicting the cell passing/trapping for IFC/EIS impedance sensing. The channels are designed following the least flow resistance path principle. IFC electrodes are underneath the main channel, and EIS electrodes are underneath the trapping sites. The first coming cell would pass the main channel for IFC and then be trapped on the trapping site for EIS. (B) Top view of the flow rate distribution in the channels. (C) Side view of the electrical model of single cell suspended in solution between electrodes. (D) Illustration of the electrical model of single cell, i.e., impedance magnitude and phase spectrum with respect to the frequency of applied excitation signals.

instance, Haandbæk et. al[24] demonstrated the ability to discriminate single and budding yeast cells and extract specific features of cells through the combination of impedance data and morphological phenotypes. EIS yields the impedance spectrum by applying a frequency-sweeping signal excitation to a trapped cell.[15] Ample single-cell trapping techniques can be incorporated into the microfluidic chip, such as DEP traps,[25] hydrodynamic traps,[26] and optical traps,[27] to trap a single cell. Many efforts like minimizing current leakage,[28] reducing serial resistance,[29] and modifying electrode surface[30] have been made to improve the measuring sensitivity.

In this study, we proposed a novel microfluidic device combining the IFC and EIS techniques, aiming to screen the electrical properties of single cells more efficiently. IFC and

EIS are both impedance-based measurement for the electrical properties of suspended cells using the same cell electrical model, which constitutes the basis for their combination. EIS can obtain the full impedance spectrum, which contains abundant characteristic information on the cell. Its low throughput may be complemented by IFC, which can promptly get several representative frequency-dependent impedance data points. The device is configured with hydrodynamic trapping sites and coplanar electrodes to allow IFC for passing cells and EIS for trapped cells. With the fabricated device, we verified the individual functionality of IFC and EIS using three types of cancer cells including HeLa, A549, and HepG2. We also demonstrated their complementarity, which holds for a wide range of flow rate. We envision
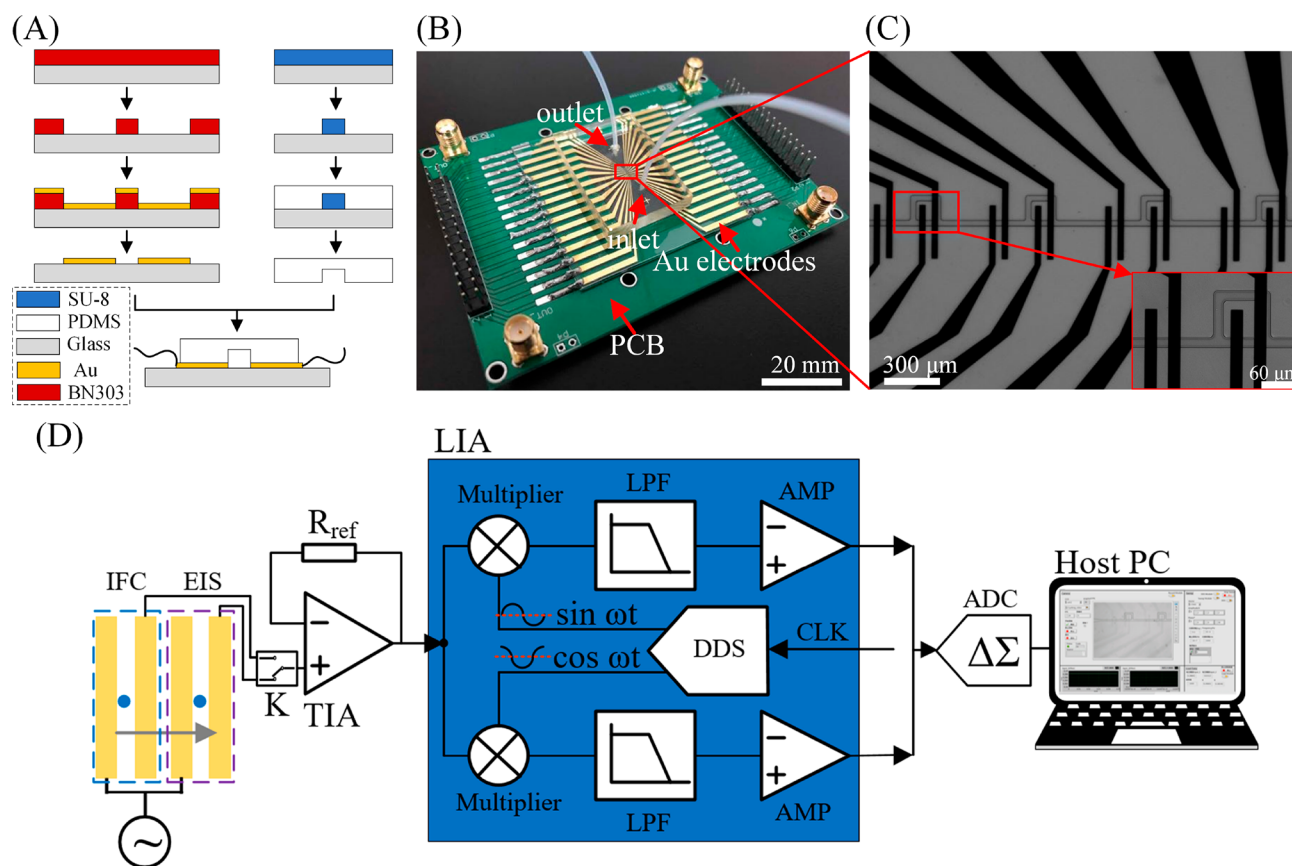
Figure 2. Microfluidic chip and the associated impedance measuring system. (A) The fabrication procedure of the microfluidic chip using the lift-off and soft-lithography technique. (B) The assembled microfluidic device composed of a PDMS top layer and a glass bottom layer patterned with electrodes which are wired out through a customized printed circuit board. (C) Optical micrograph of the chip. (D) The impedance measuring system using the principle of lock-in amplifier. The switch between IFC and EIS is controlled by a relay.

that the strategy of combining IFC and EIS provides a new thought in the efforts to enhance the efficiency of electrical property measurement for single cells.

■ WORKING PRINCIPLE

Device Design for IFC/EIS Integration. To enable EIS and IFC simultaneously, two types of microchannels are required on one chip for cells to pass or stay. One for IFC should allow the cell to pass, and the other for EIS allow the cell to stay. To this end, the device is designed with upper and lower layers (Figure 1A). The lower layer is configured with an array of coplanar electrodes for impedance sensing in IFC/EIS, while the upper layer is deployed with the two types of microchannels. According to our previous study,[31] the upper layer is designed as a passive hydrodynamic microfluidic structure with an array of repeating cell pass-and-stay units; each unit has a main channel bifurcating to two paths. The curved (bypassing) path allows for cells to pass through and the straight (trapping) path for one cell to be trapped in the narrow constriction (trapping site). Electrodes are placed properly underneath the main channel and the trapping site. The microchannel geometry of the paths ($L_1 = 125$ μm, $L_2 = 125$ μm) is designed such that the volumetric flow rate ratio of $Q_1/Q_2 > 1$ to follow the least flow resistance path principle. Under such condition, the flow resistance of the bypassing path is greater than that of the trapping path, and the first cell passing through the main channel would be trapped in the next trapping site. Therefore, the same cell can be measured via IFC

and then EIS. The number of units in this work was set to eight for demonstration purposes but can be expanded easily by tens of times through increasing the number of signal channels of the measuring system.

To achieve highly sensitive impedance sensing and avoid cell blockage and current leakage, the width and height of the microchannels are 30 μm and 20 μm respectively to allow easy passing of the cells with diameter of 10−16 μm. The constriction width is 6 μm to stop the cell fully on site for EIS. In case that the trapping site is taken up by a cell, the trapping path is presumably blocked, and its flow resistance will increase drastically so that the next pass-and-stay unit is in action (Figure 1B). In principle, the size and gap of the electrodes affect the sensitivity of measurement. The measurement signal includes three components: cell impedance, medium impedance, and double-layer impedance. Minimization of the latter two components would increase the measurement sensitivity.[32] The medium impedance is proportional to the gap of the electrodes, while the double-layer impedance is inversely proportional to the size of electrodes in direct contact with the sample solution. Thus, in practice, it is desirable to maximize the size and minimize the gap. Considering other factors such as the space efficiency, fabrication, and cell size, we set gap $g = 30$ μm, length $l = 30$ μm, and width $w = 30$ μm for the electrodes. When the cell passes through or stays on the coplanar electrodes, it replaces an equal volume of medium and thus leads to change of the impedance in the circuit. By detecting the resultant weak

difference of the response current signal via lock-in amplifier (LIA), IFC/EIS is able to measure the impedance of the cell (Impedance Measurement Method, Supporting Information). For both cases, the electrical model of a single cell in suspension (Figure 1C) is used to extract the cell electrical properties from impedance.

Electrical Model of Single Cell. The common theory and model of impedance-based techniques is the electrical model of single cell. Cell can be modeled by a single-shell spherical model, where the cell membrane is represented by a dielectric shell and the interior of the cell is represented by a homogeneous conducting cytoplasm.[34] When a suspended cell is in an ac electric field, the dielectric properties of the cell can be described with the Maxwell's mixture theory.

The electrical model is shown in Figure 1C, where R_i and R_{med} represent the resistance of cell cytoplasm and surrounding medium respectively, C_{mem} and C_{med} represent the capacitance of cell membrane and surrounding medium, C_{DL} is the double-layer capacitance between the electrodes and medium, and C_s is the stray capacitance of the device. To simplify analysis, the capacitance of cytoplasm and the resistance of membrane are neglected.[35,36] The detailed description of the model is given in the Supporting Information.

With these terms, the impedance of cell−medium mixture can be calculated as

$$Z_{mix}^* = \frac{R_{med}(1 + j\omega R_i C_{mem})}{j\omega R_{med}C_{mem} + (1 + j\omega R_i C_{mem})(1 + j\omega R_{med}C_{med})} \quad (1)$$

where ω is the angular frequency of the excitation signal. Considering C_s and C_{DL}, the overall impedance can be given by

$$Z_{theory}^* = \frac{2 + j\omega C_{DL}Z_{mix}^*}{j\omega C_{DL} + 2j\omega C_s - \omega^2 C_{DL}C_s Z_{mix}^*} \quad (2)$$

As a general example, Figure 1D illustrates the impedance spectrum of the electrical model. At low frequency ($10−10^4$ Hz), the impedance is determined mainly by C_{DL}, but the effect of C_{DL} decreases exponentially as the frequency increases. At high frequency ($10^7−10^9$ Hz), the effect of stray capacitance (C_s) becomes apparent and could be remedied by the technique of complementary metal oxide semiconductor.[29] Therefore, so far, the majority of impedance measurement works have used the medium frequency range of $10^4−10^7$ Hz, in which R_i and C_{mem} become dominant and thus accessible. Typically, the electrical properties of the cell are represented by four parameters, namely ε_i, σ_i, ε_{mem}, and σ_{mem}. They can be extracted by minimizing the squares between the measured impedance Z_{exp}^* and its model-estimated value Z_{theory}^* via

$$\min_i \Sigma [Z_{exp}^*(\omega_i) - Z_{theory}^*(\omega_i)]^2 \quad (3)$$

where i indexes the experimental data points. Note that ε_i and σ_{mem} are negligible because they make little change to the impedance spectrum in the medium frequency range. In practice, they can be assigned a reasonable value[34] to facilitate the calculation of the other two parameters.

■ MATERIALS AND METHODS

Device Fabrication. Figure 2A illustrates the fabrication procedure of the device. The microfluidic chip is composed of lower and upper layers. The lower layer is deposited with electrodes for impedance sensing, while the upper layer has PDMS microchannels for sample streaming and single-cell capture. The upper layer was fabricated using soft-lithography technique. Its brief process was the following. First, cleaned and dried glass was spin-coated with negative photoresist SU-8 2025 (MicroChem) at 4000 rpm, resulting in a photoresist film with a thickness of ∼20 μm. After soft-baking (95 °C, 5 min), UV exposure (6.9 mJ/cm², 32.6 s), and postbaking (65 °C, 1 min and 95 °C, 5 min), the photoresist was developed at room temperature to obtain the master mold. PDMS (Sylgard 184, Dow Corning) was then used for replicate. A mixture of base and curing agent (10:1 ratio by weight) was prepared, degassed, and then poured onto the master mold. After curing at 60 °C for at least 3 h, the solidified PDMS was peeled off from the mold and cut into pieces. The lower layer was fabricated through lift-off technique. Negative photoresist BN303-30 (Kempur Corp, China) was spin-coated on the clean glass and then photo patterned. Then 10 nm of Cr and 100 nm of Au were subsequently sputtered on the patterned glass. Degumming agent was utilized to remove the photoresist and left the patterned electrodes. The two layers were treated with oxygen plasma and bonded together. The assembled microfluidic device was baked at 120 °C for 1 h to further improve bonding strength ultimately. A matching printed circuit board was made to connect the electrodes for electrical signal excitation and recording. The overview of the fabricated device and corresponding microscopic image are shown in Figure 2B and Figure 2C, respectively.

Measuring Circuit Design. Figure 2D illustrates the schematic diagram of a homemade portable measuring circuit based on the LIA principle of impedance measurement.[33] The TIA was implemented by using high gain bandwidth, low bias-current, and low offset-voltage operational amplifiers (TI, OPA657). Considering the impedance variation range ($10−10^3$ kΩ) and characteristics of the amplifier, the feedback resistor of the TIA was selected as 100 kΩ. The voltage signal converted from current by the TIA was then modulated with the quadrature signal respectively using the wideband four quadrant voltage output multiplier (ADI, AD835). The modulation voltage signal was demodulated subsequently utilizing the high-precision, low-noise operational amplifiers (TI, OPA227) which served as LPF. The cutoff frequency of the LPF was selected as 10 Hz to filter out the up-converting signal with 10^3 Hz as the minimum sweeping frequency. The filtered dc voltage was then amplified (TI, OPA227) 4× to improve the signal-to-noise ratio and read by the computer through the data acquisition system (National Instruments, PCI-6289).

Cell Preparation. Cancer cells HeLa, HepG2, and A549 were cultured using an incubator (Forma 381, Thermo Scientific, USA) at 37 °C in 5% CO_2. The culture medium was the high-glucose Dulbecco's Modified Eagle's Medium (DMEM, Life technologies, USA), supplemented with 10% fetal bovine serum (FBS, Life technologies, USA) and 1% penicillin-streptomycin (Life technologies, USA). The adherent cells were detached with 0.05% trypsin (Life technologies, USA), followed by centrifuging at 300g for 5 min to remove the supernatant. Finally, the collected cells were resuspended in phosphate-buffered saline (PBS, pH 7.4) solution supplemented with 1% BSA to avoid adhesion and shaken gently to obtain the uniform cell suspension for conducting the electrical impedance measurement. A cell concentration of 10^6/mL was used in experiment.
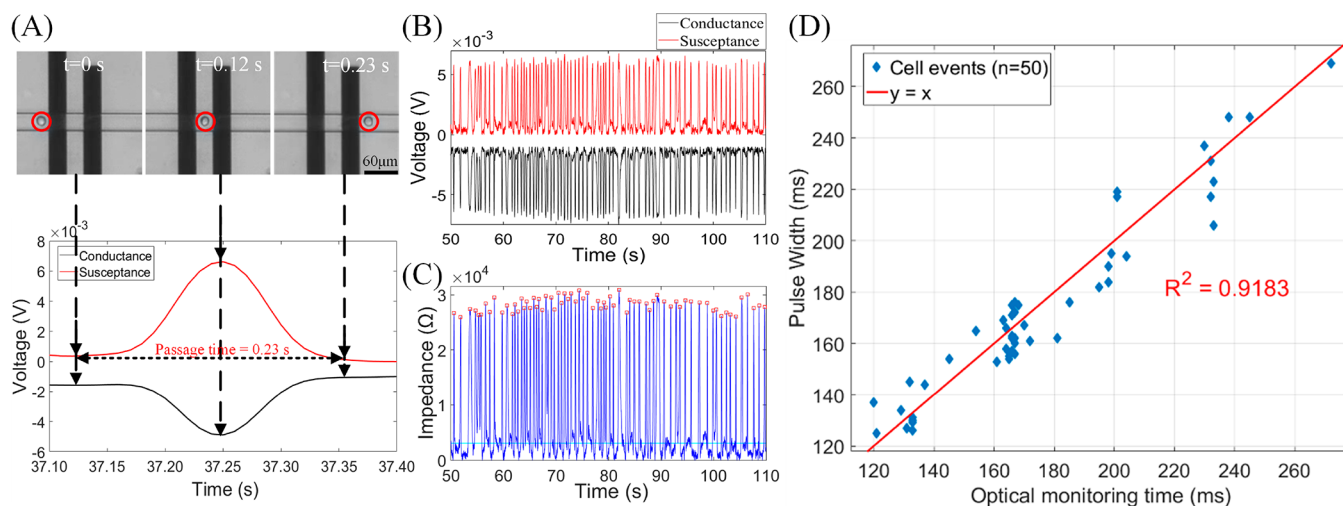
Figure 3. IFC functionality verification. (f = 1 MHz, V_{p-p} = 1 V). (A) The time-lapsed microscopic image snapshots of a HeLa cell flowing through the IFC electrodes. The corresponding electrical impedance signal of this cell transit event is illustrated below. (B) Instantaneous time-varying pulse signals measured for continuous cell transit events. (C) The corresponding impedance magnitude signal for the cell transit events in (B). The blue line represents the baseline for peak detection, and the red points highlight the pulse peaks representing a cell event. (D) The passage time measured via the microscopic video clip vs the electrical pulse width. Data points can be fitted linearly (R^2 = 0.9183).

Experimental Setup and Data Analysis. The device was placed on an inverted microscope (Ti–U, Nikon) with enough working space for electrical and fluidic circuits. A commercial signal generator (AFG3052C, Tektronix) and the homemade measuring circuit were connected to the electrodes for excitation and signal read-out, respectively. Before sample loading, the microchannel was pretreated with 1% BSA (in 1× PBS) to prevent adhesion of samples from PDMS sidewalls. Samples were subsequently loaded by pulling the syringe pump (Legato 200, KD Scientific) into the microchannel. The inputs of the IFC and the EIS sensing electrodes were applied with 1 V_{p-p}, 1 MHz and 1 V_{p-p} sweep ($1-10^3$ kHz) signals respectively, and the output of the sensing electrodes was connected to the impedance measuring system via relays (G5 V, OMRON). Note the voltage was chosen such that the ac-induced transmembrane potential was far below the threshold value (i.e., 1 V) for cell electroporation.[37] The electrical impedance data generated by the measuring circuit were acquired utilizing homemade LabVIEW program (National Instruments, USA) and analyzed via MATLAB (Math Works, USA). During the measurement process, the cell movement was recorded at 100 Hz by a CCD camera (DS-Ri1, Nikon) mounted on the microscope C-port. The video clips were synchronized with the electrical signal via time stamping and can be analyzed offline to correlate the electrical data with microscopic observation.

■ RESULTS AND DISCUSSION

Measuring System Calibration and Verification. The measuring system was calibrated using a standard resistor whose resistance is equal to the feedback resistance at a fixed frequency, according to literature.[33] Under this setting, the ideal system response is supposed to be the measured voltage equal to the input voltage (V_{out} = V_{in}). We fed into a series of input voltage and obtained corresponding output voltage values. A significant linear relationship (V_{out} = 0.9249V_{in} + 0.1488, R^2 = 0.9999) between them was confirmed (Figure S1A, Supporting Information). The calibration curves for other frequencies were also obtained with the same method and high

R-square values to facilitate measurement correction in the following experiments.

Then to verify the feasibility of the homemade measuring system, a RC network was connected to the measuring system to test the frequency response. The RC network consisting of a 100 kΩ resistor and a 13 pF capacitor was applied with a sweep signal from 10^2 to 10^6 Hz, and the impedance magnitude was calculated with the calibrated system. The excellent match (R^2 = 0.9395) between the theoretical and experimental results (Figure S1B, Supporting Information) verifies that this homemade impedance analysis system is accurate and therefore can be used for the following single-cell impedance measurement.

Impedance Flow Cytometry Validation and Classification of Cell Types. We first verified that the IFC module worked for the passing cells. For proof, HeLa cells were pulled into the channel at 10 nL/min (or 0.278 mm/s). During this course, the image frames for passing cells and the corresponding electrical impedance signal of each cell transit event were obtained (Video S1, Supporting Information). For each cell passing through the IFC electrode, the voltage signals exhibited a Gaussian shape, whose peak appeared when the cell was midway between the electrodes (Figure 3A). According to the impedance sensing mechanism, the real part of the impedance signal reflects the conductance, while the imaginary part reflects the susceptance. Compared to the no-cell case, the appearance of a cell in between the electrodes led to a decrease (valley) in conductance and increase (peak) in susceptance, because the capacitive cell membrane isolates the conductive cytoplasm from the suspending medium.[38] In continuous flowing, each peak in the impedance magnitude corresponds to a passing cell. Recording of the IFC signals (Figure 3B) for a flowing cell population has been successful to identify all pulse peaks, which were used to resolve the impedance for the passing cells (Figure 3C) at certain frequency. We also extracted the passage time for each cell event from the video clip and compared it to the pulse width extracted from the continuous IFC signals (Figure 3D). The high correlation (R^2
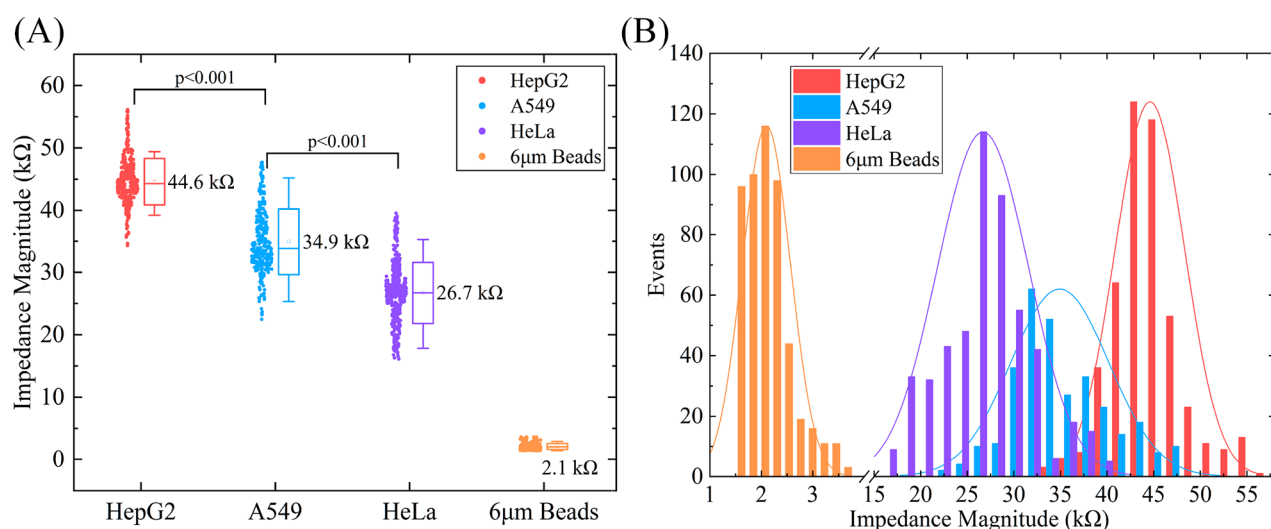
Figure 4. Impedance magnitude distribution for three types of cancer cells and 6 μm beads. (A) The average impedance magnitudes of HepG2, A549, HeLa cells and beads are 44.6 ± 10.9, 34.9 ± 12.6, 26.6 ± 11.7, and 2.1 ± 1.1 kΩ (N = 469, 351, 513, and 550, respectively), showing significant difference (p < 0.001). (B) The impedance magnitudes of cells and beads exhibit Gaussian distribution in population.
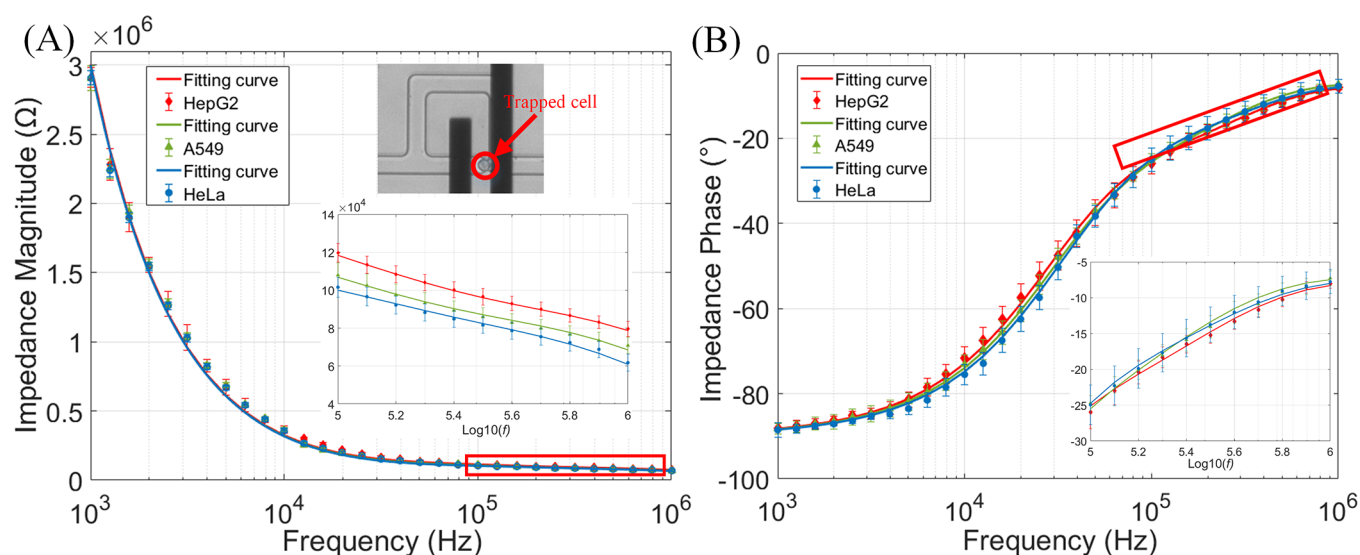

Figure 5. EIS impedance measurement results for three types of cancer cells. (A) Impedance magnitude and (B) phase spectrum. Discrete data points with standard deviation (N = 10) were obtained via EIS for the trapped cell and fitted by the curve with least error according to eq 3. Insets zoom in the high-frequency range data points.

= 0.9183) indicates that the electrical measurement is accurate and reliable.

We also demonstrated that the IFC module could work to classify different cell types. Herein, three populations of cancer cells (HepG2, A549, and HeLa) and 6 μm microbeads were independently measured via IFC. The microbeads were used as a reference group because they are of rather uniform material and size distribution. The impedance measurement was carried out at 1 MHz frequency where the overall impedance of the single cell is dominated by size and electrical property.[39] Significant differences among them (p < 0.001, based on a Mann−Whitney test, Figure 4A) were observed. The average impedance magnitudes of HepG2, A549, HeLa cells and microbeads were 44.6 ± 10.9, 34.9 ± 12.6, 26.7 ± 11.7, and 2.1 ± 1.1 kΩ (N = 469, 351, 513, and 550, respectively). Each population showed a Gaussian distribution in the impedance magnitude (Figure 4B), which was in accordance with the

report.[40] Therefore, different cell populations can be separated due to the difference of IFC-related impedance magnitude, which is associated with the size and electrical properties such as cytoplasm conductivity and membrane permittivity.

Cell may aggregate in the medium, causing some unwanted effects, for example, channel blockage or non-single-cell transit events in impedance measurement. We took three measures to consider and solve the problem. (i) Cell medium was filtered out by the cell strainer (40 μm, Corning) before experiment. (ii) The device was configured with an array of pillars with 30 μm gap as on-chip filter in the upstream of microchannels. (iii) We judged the cell transit events as non-single-cell events if the signal amplitude exceeded the average value by 50%. In experiment, therefore, we did not experience channel blockage and minimized the probability of counting multi-single-cell transit events.

Electric Impedance Spectroscopy Validation and Electrical Property Extraction. The device has been used to successfully trap single cells at the trapping sites and perform EIS measurement (Video S2, Supporting Information). In this experiment, the three types of cancer cells were also used. A sweep signal excitation was applied to the EIS electrodes, and the impedance spectrum was obtained to resolve the electrical properties via the electrical model following eq 3. Figure 5 shows the impedance magnitude and phase spectrum of the single cells, including the experimental data points and the optimized fitting curve based on the single-cell electrical model following eq 2. Experimental data points represent the average value of 10 single cells, and the error bars represent the standard deviation, which shows the heterogeneity intrinsic to the cells.

Using eqs 1−3, by setting the values of medium permittivity ε_{med}, cytoplasm permittivity ε_i, and cell membrane thickness d in accordance with their representative values from literature[35,39] and the values of double-layer capacitance C_{DL}, stray capacitance C_s, medium conductivity σ_{med}, and radius R of the cell from measurement (Supporting Information) as shown in Table 1, the electrical parameters (cytoplasm conductivity σ_i

Table 1. Electrical Model Parameters Used for EIS-Based Electrical Property Extraction

model parameters	values
double-layer capacitance C_{DL}	90 pF
stray capacitance C_s	0.5 pF
medium conductivity σ_{med}	1.515 S/m
medium relative permittivity ε_{med}	78
cytoplasm relative permittivity ε_i	60
membrane thickness d	10 nm
cell radius R	7.5 μm

and specific membrane capacitance C_{mem}) were extracted and are shown in Table 2. The extracted electrical parameter values were in agreement with literature,[18] which validates the accuracy of this method.

Table 2. EIS-Extracted Electrical Properties for Three Types of Cancer Cells

cell type	C_{mem} (mF/m^2)	σ_i (S/m)
HeLa	18.06 ± 1.12	0.38 ± 0.09
A549	24.31 ± 1.43	0.36 ± 0.12
HepG2	21.78 ± 0.96	0.32 ± 0.07

EIS and IFC Complement under the Influence of Flow Rate. After verifying the feasibility of both IFC and EIS modules, we conducted experiment to show that EIS and IFC can complement each other. In experiment, a cell passing through the main channel was first conducted with IFC. Due to the limitation of our customized circuit that only one frequency was applied at once in IFC, we pulled slowly the same cell back and forth around the IFC electrodes a few (i.e., six) times. Each time an increasing frequency was applied as the excitation, and thus we obtained six IFC-based impedance data points. Note the frequency range was selected at the high end as explained earlier in Section 2. The same cell was then pulled forward to be trapped on the trapping site for EIS measurement. For EIS measurement, we conducted several test runs with an increasing flow rate of 10 nL/min (or 0.278 mm/

s), 100 nL/min (2.78 mm/s), and 1000 nL/min (27.8 mm/s), respectively, which would generate increasing fluidic pressure on the trapped cell under EIS. In each run, the flow rate was maintained constant, and the cell impedance was measured via the EIS module described in Section 4.3, i.e., by sweeping the frequency in the range of 10^3−10^6 Hz. For proof, HeLa cells were used in the experiment. We obtained the impedance magnitude (Figure 6A) and phase spectrum (Figure 6B), respectively. Compared to the IFC results, the deviation was less than 5% for both magnitude and phase. This small value, probably caused by the trapping site associated electric field change, indicates that the IFC results can be actually a subset of EIS results. Comparing only the EIS results of the three levels of flow rate, we observed that the impedance magnitude change associated with 100 and 1000 nL/min was less than 1% and 5%. respectively, with respect to 10 nL/min. This means that in practice, we can maximize the flow rate to increase the measurement throughput of IFC module while still obtaining high accuracy.

To further test the extreme effect of the flow rate, we conducted the EIS experiment in which the flow rate was increased from 10 nL/min to 10 μL/min, which was high enough to squeeze the cell out of the trapping site. We obtained the corresponding impedance magnitude and phase at 1 MHz during this course (Figure 6C). The fluctuation of impedance was almost zero at 10 nL/min but subject to a highly dynamic change in response to the 1000× increase in flow rate (Video S3, Supporting Information). The extreme change occurred at the time being of the cell escaping from the trapping site. Therefore, as long as the cell maintains its morphology, which corresponds to a wide range of flow rate, EIS measurement results can be highly stable. Overall, IFC and EIS results can complement each other, which provides the evidence that discrete multifrequency impedance data measured by the IFC can also be used to extract cell electrical property.

It is important to point out that the main aim of the study was to test a single cell rather than a single-cell population for its both IFC and EIS results. So we decided to test the *same* cell six times, each time with a different frequency (e.g., 1 MHz, 2 MHz, ...) in IFC. In addition, our homemade measuring system is currently only able to obtain one single-frequency data point, so the same cell was driven back and forth "manually" over the electrodes six times to obtain multifrequency (six single-frequency) data points in IFC. This manual back-and-forth operation could be eliminated if multifrequency data points can be obtained simultaneously via more sophisticated instruments such as HF2IS, FPGA, or MCU.

It is also worth noting that the device can be applied in a single-cell study even with the current measurement system. For example, set the frequency to 1 MHz for IFC, run the experiment with 8 single cells automatically. In the following round, run 8 new single cells at 2 MHz and repeat the same experiment, and then the same procedure at 3 MHz and so forth. This batch measurement method at single-cell level would be effective to collect the data for cell population.

The number of measurement units is limited by the number of measurement channels of the impedance measuring system. Currently, our homemade measuring system was able to provide 8 signal channels for measurement; thus, the measurement units was set to 8. To break this limit, the measuring system can be possibly upgraded with more
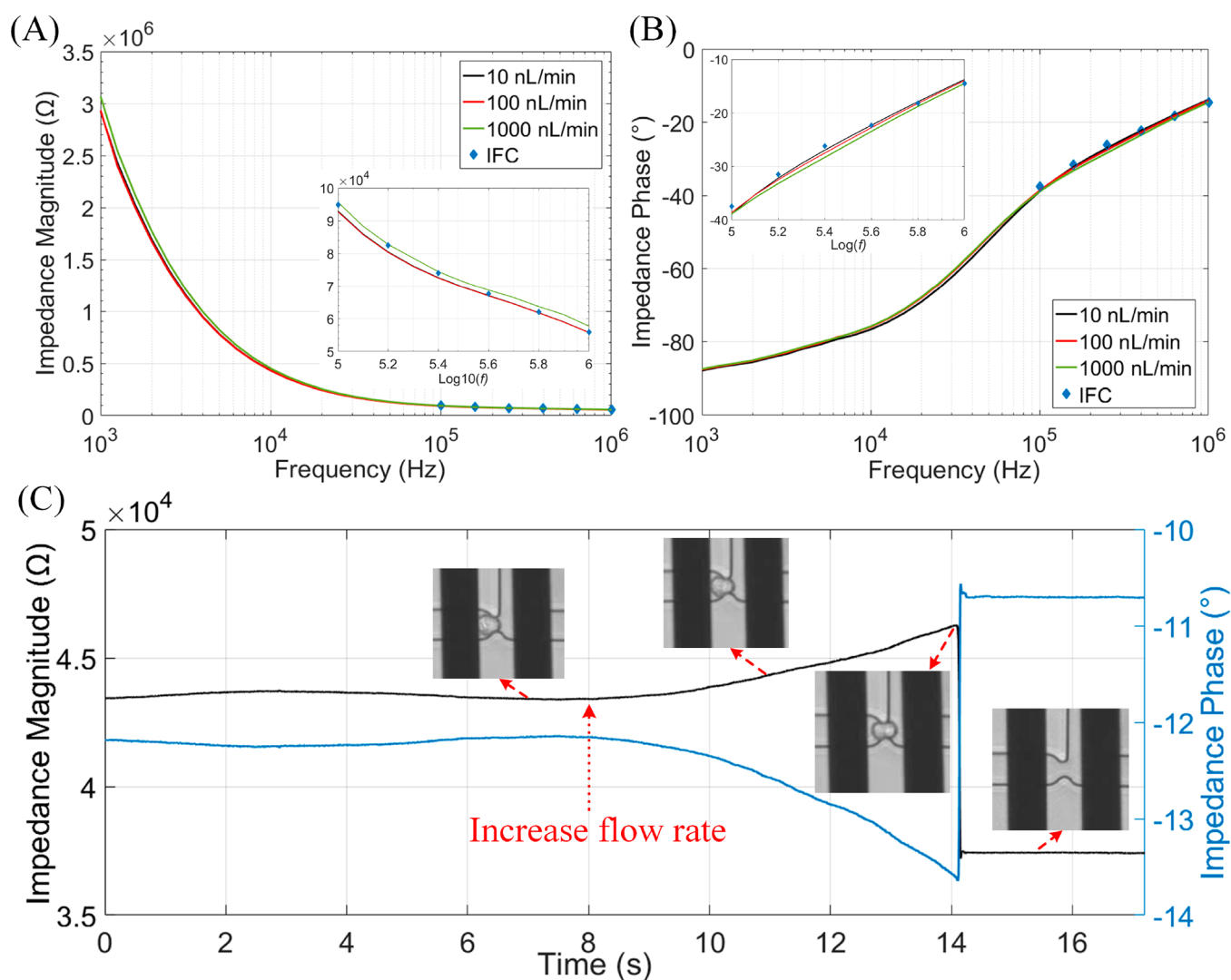
Figure 6. Comparison of the IFC results and EIS results for the same cell under the effect of flow rate. (A) Impedance magnitude and (B) phase spectrum at three levels of flow rate. Note the discrete data points are IFC results and the curves are fitting EIS results. Insets zoom in the high-frequency range data points. (C) The dynamic response of EIS-based impedance magnitude and phase when the flow rate was kept as 10 nL/min for a while and then increased to 10 μL/min ($f = 1$ MHz).

advanced analog multiplexer (e.g., TI, CD 4067B, 16-channel) integrated in the printed circuit board in series (N), such that the number of signal channels reaches $16N$. There might be challenging for N to be very big but quite normal to be at a scale of 10. Therefore, the number of measurement units can be easily reach the scale of ~200 without incurring significant extra cost in hardware components.

CONCLUSION

In this work, we combined the IFC and EIS modules into one microfluidic chip. In doing so, we applied least flow resistance path principle to trap cells, designed and fabricated the microfluidic device configured with coplanar electrodes for IFC and EIS, made a customized impedance measurement system, conducted experiment to verify individual functionality of IFC and EIS, and demonstrated the complementarity of IFC and EIS under the effect of flow rate. The device has been successful to allow cell to pass for IFC measurement and to trap for EIS measurement. Three cancer cell types were found to have significant difference in impedance magnitude by IFC, and single cells' full impedance spectrum by EIS was used to

extract the cytoplasm conductivity and specific membrane capacitance. For the same cell, the deviation of IFC from EIS was found to be less than 5% in response to a range of 3 orders of magnitude of flow rate, demonstrating that IFC measurement results were a subset of EIS results. It was also found that EIS kept almost constant in response to the wide range of flow rate, as long as the trapped cell was subject to gentle fluidic drop-induced deformation. Overall, we believe that the strategy of combining EIS and IFC offers a new approach in enhancing the efficiency of electrical property measurement for single cells.

ASSOCIATED CONTENT

Ⓢ Supporting Information

The Supporting Information is available free of charge on the ACS Publications website at DOI: 10.1021/acs.anal-chem.9b04083.

Impedance measurement method; detailed description of the electrical model of single cell; measurement methods for key parameters of the electrical model;

impedance measuring system calibration and verification results (PDF)

Video demonstrating the measuring process of IFC (AVI)

Video demonstrating the measuring process of EIS (AVI)

Video demonstrating the dynamic impedance response of the squeezed cell (AVI)

■ AUTHOR INFORMATION

Corresponding Author
*E-mail: wwh@tsinghua.edu.cn.

ORCID ⊚
Wenhui Wang: 0000-0002-5884-6098

Notes
The authors declare no competing financial interest.

■ REFERENCES

(1) Klein, A. M.; Mazutis, L.; Akartuna, I.; Tallapragada, N.; Veres, A.; Li, V.; Peshkin, L.; Weitz, D. A.; Kirschner, M. W. *Cell* **2015**, *161*, 1187−1201.

(2) Galler, K.; Brautigam, K.; Grosse, C.; Popp, J.; Neugebauer, U. *Analyst* **2014**, *139*, 1237−1273.

(3) Mansor, M. A.; Ahmad, M. R. *Int. J. Mol. Sci.* **2015**, *16*, 12686−12712.

(4) Carey, T. R.; Cotner, K. L.; Li, B.; Sohn, L. L. *Wiley Interdiscip. Rev. Nanomed. Nanobiotechnol.* **2019**, *11*, e1529.

(5) Katsumoto, Y.; Tatsumi, K.; Doi, T.; Nakabe, K. *Int. J. Heat Fluid Flow* **2010**, *31*, 985−995.

(6) Tang, W.; Tang, D.; Ni, Z.; Xiang, N.; Yi, H. *Anal. Chem.* **2017**, *89*, 3154−3161.

(7) Adamo, A.; Sharei, A.; Adamo, L.; Lee, B.; Mao, S.; Jensen, K. F. *Anal. Chem.* **2012**, *84*, 6438−6443.

(8) de Wagenaar, B.; Dekker, S.; de Boer, H. L.; Bomer, J. G.; Olthuis, W.; van den Berg, A.; Segerink, L. I. *Lab Chip* **2016**, *16*, 1514−1522.

(9) Asphahani, F.; Zhang, M. *Analyst* **2007**, *132*, 835−841.

(10) Srinivasaraghavan, V.; Strobl, J.; Agah, M. *Lab Chip* **2012**, *12*, 5168−5179.

(11) Arias, L. R.; Perry, C. A.; Yang, L. *Biosens. Bioelectron.* **2010**, *25*, 2225−2231.

(12) Vembadi, A.; Menachery, A.; Qasaimeh, M. A. *Front. Bioeng. Biotechnol.* **2019**, *7*, 147.

(13) Shrirao, A. B.; Fritz, Z.; Novik, E. M.; Yarmush, G. M.; Schloss, R. S.; Zahn, J. D.; Yarmush, M. L. *Technology* **2018**, *6*, 1−23.

(14) Jain, G.; Muley, N.; Soni, P.; Singh, J. N.; Sharma, S. S. *Curr. Res. Inf. Pharm. Sci.* **2009**, *10*, 9−15.

(15) Xu, Y.; Xie, X.; Duan, Y.; Wang, L.; Cheng, Z.; Cheng, J. *Biosens. Bioelectron.* **2016**, *77*, 824−836.

(16) Zheng, Y.; Nguyen, J.; Wei, Y.; Sun, Y. *Lab Chip* **2013**, *13*, 2464−2483.

(17) Nguyen, T. A.; Yin, T. I.; Reyes, D.; Urban, G. A. *Anal. Chem.* **2013**, *85*, 11068−11076.

(18) Huang, L.; Zhao, P.; Wang, W. *Lab Chip* **2018**, *18*, 2359−2368.

(19) Huang, L.; He, W.; Wang, W. *Electrophoresis* **2019**, *40*, 784−791.

(20) Hughes, M. P. *Phys. Med. Biol.* **1998**, *43*, 3639.

(21) Bull, B. S.; Schneiderman, M. A.; Brecher, G. *Am. J. Clin. Pathol.* **1965**, *44*, 678−688.

(22) Rodriguez-Trujillo, R.; Castillo-Fernandez, O.; Garrido, M.; Arundell, M.; Valencia, A.; Gomila, G. *Biosens. Bioelectron.* **2008**, *24*, 290−296.

(23) Holmes, D.; Pettigrew, D.; Reccius, C. H.; Gwyer, J. D.; van Berkel, C.; Holloway, J.; Davies, D. E.; Morgan, H. *Lab Chip* **2009**, *9*, 2881−2889.

(24) Haandbæk, N.; Bürgel, S. C.; Rudolf, F.; Heer, F.; Hierlemann, A. *ACS Sens.* **2016**, *1*, 1020−1027.

(25) Mansoorifar, A.; Koklu, A.; Beskok, A. *Anal. Chem.* **2019**, *91*, 4140−4148.

(26) Mi, L.; Huang, L.; Li, J.; Xu, G.; Wu, Q.; Wang, W. *Lab Chip* **2016**, *16*, 4507−4511.

(27) Lai, C.-W.; Hsiung, S.-K.; Yeh, C.-L.; Chiou, A.; Lee, G.-B. *Sens. Actuators, B* **2008**, *135*, 388−397.

(28) Zhao, Y.; Wang, K.; Chen, D.; Fan, B.; Xu, Y.; Ye, Y.; Wang, J.; Chen, J.; Huang, C. *Biosens. Bioelectron.* **2018**, *111*, 138−143.

(29) Chien, J. C.; Ameri, A.; Yeh, E. C.; Killilea, A. N.; Anwar, M.; Niknejad, A. M. *Lab Chip* **2018**, *18*, 2065−2076.

(30) Guo, X.; Zhu, R.; Zong, X. *Analyst* **2015**, *140*, 6571−6578.

(31) Jin, D.; Deng, B.; Li, J. X.; Cai, W.; Tu, L.; Chen, J.; Wu, Q.; Wang, W. H. *Biomicrofluidics* **2015**, *9*, 014101.

(32) Cottet, J.; Kehren, A.; van Lintel, H.; Buret, F.; Frénéa-Robin, M.; Renaud, P. *Microfluid. Nanofluid.* **2019**, *23*, DOI: 10.1007/s10404-018-2178-6

(33) Zhen, C.; Xie, X.; Xu, Y. *2015 IET International Conference on Biomedical Image and Signal Processing (ICBISP)*, 2015; 7 pp.

(34) Sun, T. A. O.; Green, N. G.; Morgan, H. *Nano* **2008**, *03*, 55−63.

(35) Morgan, H.; Sun, T.; Holmes, D.; Gawad, S.; Green, N. G. J. *J. Phys. D: Appl. Phys.* **2007**, *40*, 61−70.

(36) Sun, T.; Green, N. G.; Gawad, S.; Morgan, H. *IET Nanobiotechnol.* **2007**, *1*, 69−79.

(37) Kinosita, K.; Tsong, T. Y. *Biochim. Biophys. Acta, Biomembr.* **1977**, *471*, 227−242.

(38) Huang, C.; Chen, A.; Guo, M.; Yu, J. *Biotechnol. Lett.* **2007**, *29*, 1307−1313.

(39) Carminati, M.; Ferrari, G.; Vahey, M. D.; Voldman, J.; Sampietro, M. *IEEE Trans. Biomed. Circuits Syst.* **2017**, *11*, 1438−1449.

(40) Zhou, Y.; Yang, D.; Zhou, Y.; Khoo, B. L.; Han, J.; Ai, Y. *Anal. Chem.* **2018**, *90*, 912−919.